Contrast-Enhanced Near-Infrared Optical Imaging Detects Exacerbation and Amelioration of Murine Muscular Dystrophy

Stephen M. Chrzanowski, PhD[1], Ravneet S. Vohra, PT, PhD[1],
Brittany A. Lee-McMullen, PhD[2], Abhinandan Batra, PT, MA, PhD[3],
Ray A. Spradlin, BS[4], Jazmine Morales, BS[4], Sean Forbes, PhD[3],
Krista Vandenborne, PT, PhD[3], Elisabeth R. Barton, PhD[4], and
Glenn A. Walter, PhD[1]

Abstract

Assessment of muscle pathology is a key outcome measure to measure the success of clinical trials studying muscular dystrophies; however, few robust minimally invasive measures exist. Indocyanine green (ICG)-enhanced near-infrared (NIR) optical imaging offers an objective, minimally invasive, and longitudinal modality that can quantify pathology within muscle by imaging uptake of ICG into the damaged muscles. Dystrophic mice lacking dystrophin (mdx) or gamma-sarcoglycan (Sgcg$^{-/-}$) were compared to control mice by NIR optical imaging and magnetic resonance imaging (MRI). We determined that optical imaging could be used to differentiate control and dystrophic mice, visualize eccentric muscle induced by downhill treadmill running, and restore the membrane integrity in Sgcg$^{-/-}$ mice following adeno-associated virus (AAV) delivery of recombinant human SGCG (desAAV8hSGCG). We conclude that NIR optical imaging is comparable to MRI and can be used to detect muscle damage in dystrophic muscle as compared to unaffected controls, monitor worsening of muscle pathology in muscular dystrophy, and assess regression of pathology following therapeutic intervention in muscular dystrophies.

Introduction

Phenotypically, the muscular dystrophies are defined by a common clinical presentation of progressive, degenerative, and irreversible muscle weakness.[1] With the advent of modern sequencing technologies, over 50 genetically unique forms of muscular dystrophy have been identified.[2] The most common form of muscular dystrophy in children is Duchenne muscular dystrophy (DMD), with an incidence of 1 in 5000 live male births.[3] Duchenne muscular dystrophy is caused by a mutation in the *dystrophin* gene, which encodes for the dystrophin protein.[4] Functional dystrophin connects the intracellular actin cytoskeleton to the dystrophin-associated glycoprotein complex (DGC), stabilizing the sarcolemmal membrane during muscle contractions.[4,5] Another form of muscular dystrophy is limb-girdle muscular dystrophy 2C (LGMD2C) resulting from mutations in the *SGCG* gene, which encodes for production of the γ-sarcoglycan.[6] As a critical component of the DGC,

γ-sarcoglycan is one of the several sarcolemmal transmembrane glycoproteins, and its absence leads to sarcolemmal fragility, as phenotypically seen in LGMD2C.[7]

Currently, few drug treatments are commercially available to treat the muscular dystrophies, though many therapies have

[1] Department of Physiology and Functional Genomics, University of Florida, Gainesville, FL, USA
[2] Department of Biochemistry, University of Florida, Gainesville, FL, USA
[3] Department of Physical Therapy, University of Florida, Gainesville, FL, USA
[4] Department of Applied Physiology and Kinesiology, University of Florida, Gainesville, FL, USA

Corresponding Author:
Glenn A. Walter, Department of Physiology and Functional Genomics, University of Florida, 1600 SW Archer Rd, M552, PO Box 100274, Gainesville, FL 32610, USA.
Email: glennw@ufl.edu

shown promise in preclinical and early clinical trials.[8-11] Two commonly studied preclinical dystrophic mouse models are the DMD (*mdx*) and LGMD2C (*Sgcg*$^{-/-}$) knockout mouse lines.[12,13] These models have been effectively used to study both diseases, as well as to develop a variety of therapies, including pharmacological interventions,[14,15] exon skipping,[16,17] viral delivery,[18] and nonsense suppression therapies.[19] Although not the ideal mouse model to study DMD, *mdx* mice are the most frequently utilized and demonstrate a large initial inflammatory cascade, followed by slower progression of disease.[20,21] *Sgcg*$^{-/-}$ mice demonstrate a more progressive phenotype, demonstrating decreased growth, premature death, and severely dystrophic muscle with aging.[12] Having biomarkers able to detect mitigation of disease or worsening of pathology is critical for a successful clinical trial. Furthermore, to date, clinical trial efficacy has been hampered by a lack of such an outcome measure; therefore, a pressing need exists for sensitive biomarkers to detect disease, further insult to dystrophic muscle, and response to potential therapies for the muscular dystrophies.

Quantifiable assessment of inducible damage and therapeutic intervention in preclinical models is limited to several modalities, including histological markers of muscle damage and *ex vivo* muscle contraction assessments.[21,22] Although clinical trials regularly use muscle biopsies, they are not ideal due to the invasive nature; therefore, minimally invasive measures are preferred. Other measures of muscle damage include assessing microRNAs, creatine kinase, and the 6-minute walk test, but these measures lack the ideal sensitivity and specificity necessary for clinical trials.[23,24] An optimal means of measuring muscle health would be applicable both to animals and humans, allowing for acceleration of preclinical findings to clinical studies. Recently, magnetic resonance imaging (MRI) has provided the ability to study disease in a longitudinal and noninvasive fashion both in humans and preclinical models.[25-30] Changes in MRI-T_2 times reflect a number of different pathological processes that occur in muscle, such as myonecrosis,[31,32] edema,[33] fatty tissue infiltration,[34] and fibrosis.[35] Although a plethora of helpful information can be gathered from MR techniques, several limitations do exist, including adequate compliance of children, metallic implant contraindications, cost, and speed of operation,[36] and thus, we propose to further develop near-infrared (NIR) optical imaging as a complementary technology to collect minimally invasive, quantitative, and repeatable information.

Contrast-enhanced NIR optical imaging recently has developed as an effective tool for several clinical applications, such as perfusion studies[37] and tumor identification.[38,39] In muscle, NIR spectroscopic techniques have previously monitored blood volume, oxygenation, and flow dynamics using fluorescent dyes.[40] Through utilization of optical imaging in the NIR range (700-1000 nm), several advantages exist when compared to operating at shorter wavelengths: deeper photon penetration within tissue and minimal autofluorescence.[41-43] However, these studies do not assess actual muscle pathology, but rather flow dynamics. A limited number of NIR optical imaging techniques have been conducted to directly assess muscle damage, first in *mdx* mice using a caged NIR cathepsin B substrate[44] and later in a rat model of muscle damage using an indocyanine green (ICG) derivative.[45] While these provide valuable information regarding the state of muscle pathology and response to therapy, clinical application of these techniques to the muscular dystrophies is limited because they do not use clinically approved NIR optical imaging contrast agents. Our group recently has investigated the potential use of unmodified ICG-enhanced NIR optical imaging as a means to detect muscle damage in healthy mice.[32] Indocyanine green is an FDA-approved fluorescent blood pooling agent which binds to albumin in circulation, and through the enhanced permeation and retention effect, it is retained in pathological tissues. We have previously shown that ICG accumulates in damaged muscle following acute muscle damage in control mice, similar to Evan's blue dye.[32] Through uptake into damaged dystrophic muscle, it is anticipated that application of the clinically approved ICG-enhanced NIR optical imaging may be able to spatially image and sensitively quantify muscle pathology. Further, we expect ICG-enhanced NIR optical imaging will be sensitive enough to detect inducible damage and amelioration of disease in mice.

The main aim of this study was to test whether ICG-enhanced NIR optical imaging can detect and quantify damage in dystrophic muscles, resulting from the natural pathological progression in 2 different muscular dystrophies (DMD and LGMD2C) *in vivo*. Furthermore, we also examined whether contrast-enhanced NIR optical imaging will be sensitive to assess exacerbation of muscle pathology by inducing an additional bout of muscle damage using a well-established model of downhill treadmill running in *mdx* mice. Finally, we tested whether NIR optical imaging could quantify and visualize the mitigation of disease burden on *Sgcg*$^{-/-}$ mice following delivery of *SGCG* via adeno-associated virus (AAV). We hypothesize that NIR optical imaging is able to sensitively detect damage to muscle secondary to natural disease processes and mitigation of the disease processes in two dystrophic mouse models.

Materials and Methods

Animal and Experimental Protocol

All studies were approved by the University of Florida's Institutional Animal Care and Use Committee, Gainesville, Florida (protocol number, 201507488). All experiments were performed in accordance with relevant guidelines and regulations. All experiments were performed in a blinded fashion and mice for experimental cohorts were randomly determined. Control C57/BL10 and C57/BL10ScSn-*Dmd*^{mdx}/J (*mdx*) mice breeding pairs were obtained from Jackson Laboratories (Bar Harbor, Maine) and thereafter bred in-house through the University of Florida's Animal Care Services. *Sgcg*^{tm1Mcn} (*Sgcg*$^{-/-}$) mice were generously provided by Dr. Elisabeth Barton. Mice were housed in Association for Assessment and Accreditation of

Laboratory Animal Care regulated facilities (12-hour light/dark cycle, 72°F, 42% humidity) and provided food ad libitum throughout the study. Data collection for each mouse included NIR optical imaging and MRI. To compare age-matched control mice to the 2 dystrophic phenotypes, data were collected in a cross-sectional fashion at 6 to 10 weeks of age (n = 8 per group). To exacerbate muscle damage on top of the dystrophic disease phenotype, treadmill experiments were performed on *mdx* mice aged 12 to 32 weeks (n = 5). Further, to assess the ability to detect mitigation of disease phenotype following treatment, AAV therapy was initiated on *Sgcg*$^{-/-}$ mice (n = 8) aged 6 to 10 weeks. Data were collected before and after the trial, including histology at the conclusion of the experiments.

Mdx mice were run on a downhill (14° decline) motorized treadmill at a speed of 8 to 10 m/min for up to 45 minutes as previously described.[31] Five minutes prior to the downhill running, mice were allowed to acclimate to the treadmill environment by running horizontally at a speed of no greater than 5 m/min. Mice were provided a short burst of compressed air behind them to encourage compliance to run up to 45 minutes. Post treadmill data collection occurred 48 hours after treadmill running. The same mice were used to collect both pretreadmill and posttreadmill data.

Human *SGCG* complementary DNA was utilized to generate recombinant AAV serotype 2/8 and expression was regulated by a truncated desmin promoter as previously described (desAAV8hSGCG).[18]. Vector production was performed at the University of Pennsylvania Vector Core. Fifty microliter (uL) of a 1:20 solution of viral particles diluted in phosphate-buffered saline (PBS) was injected in the tibialis anterior (TA) muscle and 100 μL into the gastrocnemius (Gas) muscle. Hind limbs were randomly preselected to receive the AAV therapy. Following injections, mice were housed in the animal facility for 6 weeks, after which data (MRI, NIR optical imaging, and histology) were collected.

For all mice, 1 hour prior to NIR optical imaging, NirawaveC ICG (Miltenyi Biotec Inc, San Diego, California) was intravenously administered per the package insert (1 mg ICG/kg body weight). Following an initial peak of fluorescence of the dye in the vascular compartments, a steady signal was maintained between 30 minutes and 3 hours postinjection (data not shown), and NIR optical imaging data were collected at 1 hour postinjection. Near-infrared optical image capture typically was performed in less than a minute per mouse. Mice were anesthetized using an oxygen and isofluorane mixture (3% induction, 0.75%-1% maintenance) and NIR optical imaging was performed using an in vivo fluorescence imager (field of view [FOV]: 9 × 9 cm, excitation wavelength: 745 nm, emission wavelength: 820 nm; Perkin Elmer, Waltham, Massachusetts). Acquired images were analyzed using Living Image software on the same in vivo fluorescence imager. Total radiant efficiency from all experiments was normalized to account for differences in scanning laser power, exposure times, and scanning area selected between mice.

To support NIR optical findings, MRI was performed in a 4.7-T horizontal 22.5-cm bore magnet (Agilent, Santa Clara, California) immediately following NIR optical imaging. Animals were anesthetized using an oxygen and isofluorane mixture (3% induction, 0.75%-1% maintenance) and were kept warm with a heated water tubing system for the duration of MR procedures. Respiratory rate and temperature were monitored (Small Animal Instruments, Stony Brook, New York) throughout the scans to ensure adequate physiologic maintenance while under anesthesia, and anesthesia was appropriately adjusted as needed. Limbs were inserted into a custom-built solenoid 200 MHz ^{1}H coil (2.0 cm internal diameter). To obtain correct positioning of all subsequent scans, localizer images in orthogonal planes were acquired using a gradient echo sequence (Repetition Time [TR] = 30 milliseconds, Echo Time [TE] = 5 milliseconds, slice thickness = 2 mm, slice number = 3 per plane, acquisition matrix = 128 × 128, signal averages = 1). Axial proton T_2-weighted multislice MR images were obtained along the length of all mouse forelimbs and lower hind limbs (TR = 2000 milliseconds, TE = 14 and 40 milliseconds, FOV = 10 × 20 mm^2, slice thickness = 1 mm, slice number = 12, acquisition matrix = 128 × 256, signal averages = 2). MRI-T_2 decay was calculated assuming a single exponential curve decay, based on previous work that has demonstrated the ability to differentiate healthy from damaged muscle.[21,31,32] Diffusion weighting was fixed at both TEs, and Hahn spin echoes were implemented to avoid contribution of stimulated echoes in the T_2 measurements. The MR images were converted from raw Varian format to Digital Imaging and Communications in Medicine (DICOM) files for analysis. To assess intramuscular differences, individual slices were stacked into continuous sections encompassing the entire length of the mouse lower hind limb. Each stack was analyzed individually, and a series of 3 images were used to quantify MRI-T_2 measurements, beginning 6 mm distal from the tibial plateau as the anatomical reference point, ensuring consistent measurements were performed. For all presented data, regions of interest (ROIs) were drawn to include all limb muscles, excluding bone and as much fascia as possible. Additionally, ROIs were drawn in a blinded fashion around individual muscle compartments, including the forelimb anterior and posterior compartments and the anterior, medial, and posterior compartments of the lower hind limbs. All image processing was performed using Osirix software (Geneva, Switzerland) to calculate signal intensity and T_2 relaxation times.

At the conclusion of experiments, mice were sacrificed the day following NIR optical imaging and MRI data capture. In the AAV treatment protocol, muscles (TA and Gas) were carefully dissected, fixed in Optimal Cutting Temperature at resting length, immediately frozen in isopentane precooled by liquid nitrogen, and stored at −80°C. Cryosections 10 μm were prepared from TA and Gas muscle. Sections were blocked with 5% bovine serum albumin (BSA) in PBS for 1 hour at room temperature and incubated with a rabbit polyclonal antibody against γ-sarcoglycan (kind gift from Elizabeth McNally, Northwestern University, Chicago, Illinois, USA), diluted
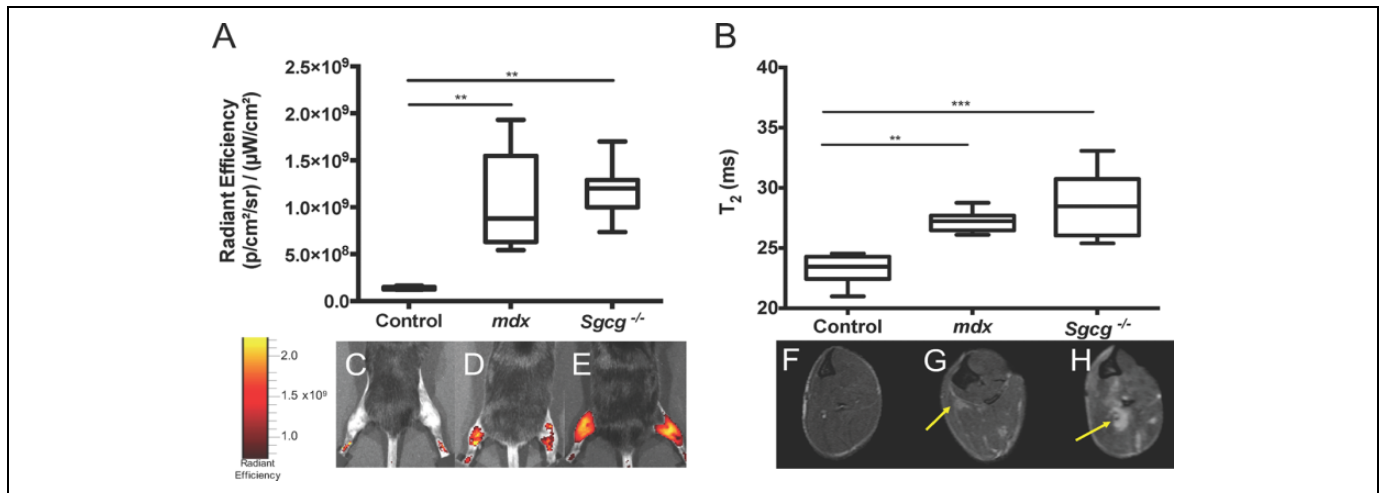
Figure 1. Dystrophic muscle can be detected by NIR optical imaging, MRI, and MRS. NIR optical imaging (1A) and MRI-T2 (1B) are able to differentiate control muscle from *mdx* and *Sgcg*$^{-/-}$ muscle. Representative NIR optical images of healthy (1C), *mdx* (1D), and *Sgcg*$^{-/-}$ (1E) mice are shown. Similarly, MR images are shown of healthy (1F), *mdx* (1G), and *Sgcg*$^{-/-}$ (1H) mice. Arrows highlight hyperintense regions in the *mdx* (1G) and *Sgcg*$^{-/-}$ (1H) mouse MRI images. Significant values (**$p < 0.01$; and ***$p < 0.001$) are indicated.

(1:500) in 5% BSA overnight at 4°C. The sections were then washed in 1× PBS to remove any excess antibody. After washing, the secondary antibody, Alexa 488 anti-rabbit (1:2000), and wheat germ agglutinin 555 conjugate (1:500; Invitrogen, Carlsbad, California) were applied to the sections and allowed to incubate for 1.5 hours at room temperature. The sections were then washed again in 1× PBS, allowed to slightly air-dry, mounted with coverslips using Vectashield with 4′,6-diamidino-2-phenylindole (DAPI) (H-1200; Vector Laboratories, Burlingame, California) as a mounting medium, sealed with clear nail polish, and stored at 4°C.

Immunoblotting was performed to quantify the amount of SGCG produced by viral injection as previously described.[18] In summary, homogenized lysates from treated and untreated muscles of *Sgcg*$^{-/-}$ mouse were probed to identify γ-sarcoglycan (1:1000 rabbit polyclonal antibody NBP1-59744; Novus Biologics, Littleton, CO, USA) and glyceraldehyde 3-phosphate dehydrogenase (GAPDH; mouse antibody sc-32233; Santa Cruz, Dallas, TX, USA). Muscles were homogenized in 10 volumes/muscle wet weight of modified lysis buffer (pH 7.4, Tris–HCl [150 mM], Triton X-100 [1% wt/vol], sodium deoxycholate [0.25%], NaCl [150 mM], phenylmethylsulfonyl fluoride [1 mM], aprotinin [1 mg/mL], leupeptin [1 mg/mL], pepstatin [1 mg/mL], NaVO$_4$ [1 mM], NaF [1 mM], and EGTA [1 mM]) and centrifuged to obtain supernatant. Protein 40 μg from each lysate was obtained, separated by 10% sodium dodecyl sulfate polyacrylamide gel electrophoresis, and transferred to polyvinylidene fluoride membranes (Millipore, Billerica, Massachusetts). Then, membranes were incubated at room temperature in Odyssey Blocking Buffer (LI-COR, Lincoln, Nebraska) for 90 minutes, followed by incubation in primary antibodies diluted in the same buffer. The next day, membranes were washed, then incubated with IRDye secondary antibodies (800cw donkey a-rabbit 925-32213, 680cw goat a-mouse 925-68070; LI-COR). Band detection and intensity

analysis was performed on an Odyssey LX imaging system and associated software (LI-COR). Membranes were finally stained with Coomassie brilliant blue R-250 to confirm equal protein loading.

All statistical analyses were performed using Prism 6.0 (GraphPad, La Jolla, California). One-way analysis of variance (ANOVA) tests were utilized to compare cross-sectional data between control and dystrophic mouse data. Standard linear regression was performed to compare NIR optical imaging to MRI-T$_2$ for all experiments. Two-way ANOVA tests with Bonferroni correction were utilized to investigate muscle damage in the treadmill and AAV experimental cohorts. Significance levels were tested at an alpha level of .05.

Results

Near-Infrared Optical Imaging Identifies Muscular Dystrophy in Mice

To determine whether NIR optical imaging can differentiate healthy from dystrophic muscle, control (n = 5, aged 12-32 weeks), *mdx* (n = 5, aged 12-32 weeks), and *Sgcg*$^{-/-}$ (n = 8, aged 6-10 weeks) mice were compared using NIR optical imaging and MRI. A significant increase of fluorescence was observed in *mdx* and *Sgcg*$^{-/-}$ mice as compared to their unaffected counterparts (Figure 1A) using ICG-enhanced NIR optical imaging. Less ICG fluorescence was visualized in control mice (Figure 1C) compared to *mdx* (Figure 1D) and *Sgcg*$^{-/-}$ (Figure 1E) strains of mice. In support of NIR optical imaging findings, MRI-T$_2$ times of the lower hind limb muscles were elevated in both dystrophic phenotypes (Figure 1B) compared to controls. Of note was the nonhyperintense uniformity of T$_2$ in control mouse muscle (Figure 1F) compared to patches highlighted by arrows in T$_2$-weighted images, indicating muscle pathology in both *mdx* (1G) and *Sgcg*$^{-/-}$ (1H) hind limbs.
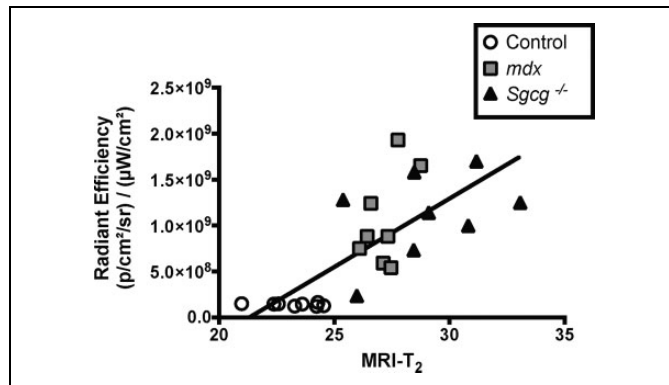
Figure 2. Increased radiant efficiency linearly correlates with increased MRI-T_2 in healthy and dystrophic mice. Dystrophic mice with increased radiant efficiency measures concurrently have elevated MRI-T_2 times ($r^2 = 0.56$, $P < 0.0001$).

Upon comparison of NIR optical imaging values to MRI relaxation times (MRI-T_2), a significant correlation was observed between these 2 parameters when all measurements from control, *mdx*, and $Sgcg^{-/-}$ mice ($r^2 = .56$, $P < .0001$; Figure 2) are considered.

Eccentric Loading by Downhill Treadmill Running Induces Quantifiable Muscle Damage in Mdx Mice

Next, to test whether NIR optical imaging was sensitive to quantify exacerbation of muscle damage in a dystrophic phenotype, a cohort of *mdx* mice underwent downhill treadmill

running. When compared to baseline values acquired before downhill treadmill running, older *mdx* mice demonstrated significant increases of measurable fluorescence in both the forelimbs and hind limbs (Figure 3A). Although MRI-T_2 relaxation times of forelimb and hind limb muscles trended to increase, only the hind limb muscles demonstrated significant changes in MRI-T_2 following treadmill running (Figure 3B). However, localized measurement of MRIs from the forelimb posterior and hind limb medial compartments demonstrated increases in MRI-T_2 (Supplement Figure), as previously reported.[32] Representative NIR optical images (Figure 3C) and MR images (3-D) images are shown. Following treadmill running, there was no significant correlation between NIR optical imaging and MRI-T_2 when using the measurements for the forelimb and hind limb muscles ($r^2 = .02$, $P > .05$; Figure 4).

Restoration of γ-Sarcoglycan in Muscle Is Observed by ICG-Enhanced NIR Optical Imaging

Quantification of disease mitigation resulting from therapeutic intervention was tested by restoring γ-sarcoglycan via AAV intramuscular injections of human *SGCG* into $Sgcg^{-/-}$ mice. Before and 6 weeks after desAAV8hGCG injections, NIR optical imaging and MRI were collected from the $Sgcg^{-/-}$ mice. Indocyanine green fluorescence was decreased significantly in the treated hind limbs compared to both preinjection values of the same hind limbs and noninjected hind limbs (Figure 5A). Similarly, MRI quantitatively demonstrated a decrease in T_2 signal in the injected hind limbs (Figure 5B). Representative NIR optical images for the baseline $Sgcg^{-/-}$ (Figure 5C) and
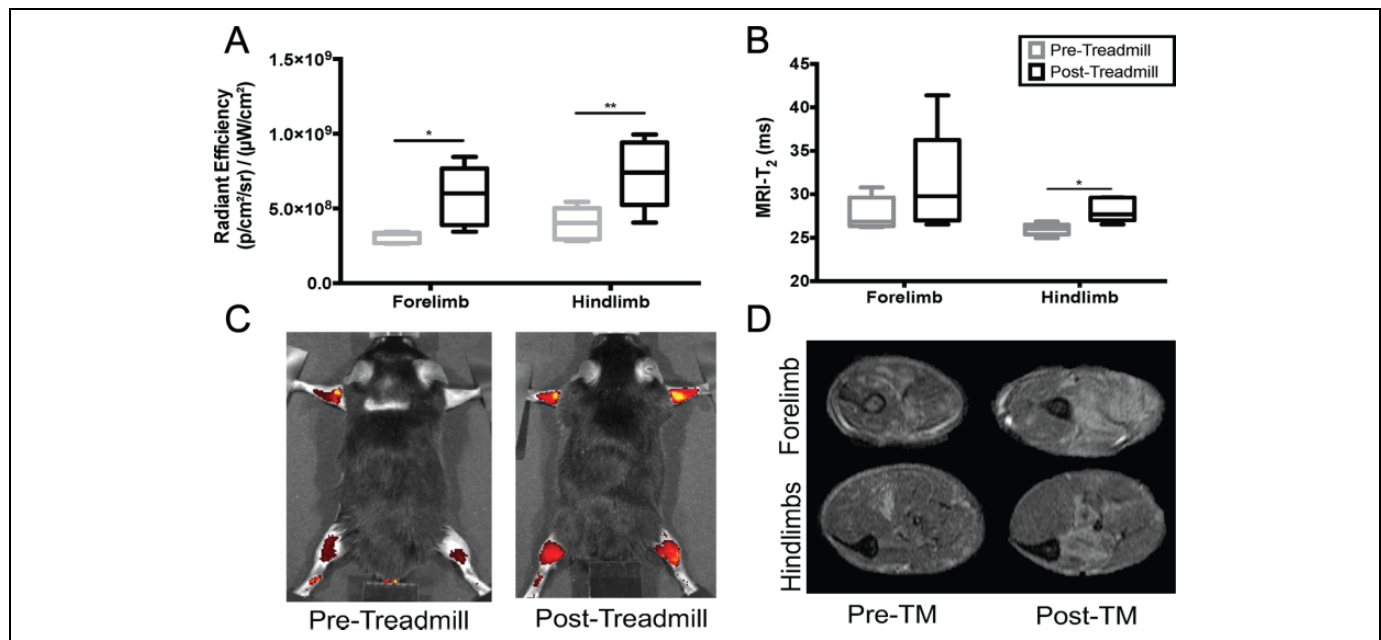
Figure 3. NIR optical imaging, but not MRI, identifies increased damage to muscle following treadmill exercising in *mdx* mice. NIR optical imaging (3A) demonstrates increased radiant efficiency following downhill treadmill running. MRI-T_2 values (3B) show no significant increase in MRI-T_2 following the treadmill exercise. NIR optical images (3C) and MR images (3D) are shown before and after treadmill running in both the forelimbs and hindlimbs. Significant values (*p < 0.05 and **p < 0.01) are indicated.
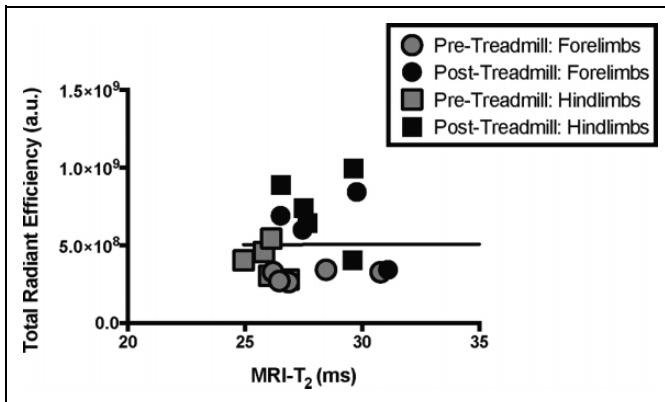
Figure 4. Increased total radiant efficiency does not correlate with increased magnetic resonance measures before and after damage induced by treadmill running. Mice with increased radiant efficiency did not correlate to elevated MRI-T_2 ($r^2 = 0.02$, $p > 0.05$) times by whole muscle assessment.

to-be-treated $Sgcg^{-/-}$ (Figure 5D) mice, as well as +6-week images of nontreated $Sgcg^{-/-}$ (Figure 5E) and treated $Sgcg^{-/-}$ (Figure 5F) mice are shown. Confirming the NIR optical imaging findings, MRI-T_2 (Figure 5B) demonstrated similar trends of decreased muscle damage in the treated hind limbs. Similarly, representative MRI images highlighting hyperintense regions of pathology are shown on baseline $Sgcg^{-/-}$ (Figure 5G) and to-be-treated $Sgcg^{-/-}$ (Figure 5H) mice, as well as + 6-week images of nontreated $Sgcg^{-/-}$ (Figure 5I) and treated $Sgcg^{-/-}$ (Figure 5J) mice. Note that the dashed gray box indicated in Figure 5A and B indicate the 95% of control values for both respective measures. Similar to the previous experiments,

correlation plots are shown comparing NIR optical imaging to MRI-T_2 ($r2 = .43$, $P < .01$; Figure 6), demonstrating correlation of radiant efficiency and MRI-T_2 in the AAV therapeutic intervention cohort.

Histological assessment confirmed that γ-sarcoglycan was restored to muscles that received *SGCG* via AAV (Figure 7). The left panel of Figure 7 shows the restoration of γ-sarcoglycan with sarcolemmal distribution throughout TA muscles that were injected, whereas the right panel of Figure 7 shows a complete lack of γ-sarcoglycan in $Sgcg^{-/-}$ muscles that did not receive treatment. Furthermore, immunoblots calculating the γ-sarcoglycan to GAPDH ratio confirmed expression of γ-sarcoglycan in the AAV-treated $Sgcg^{-/-}$ limbs, as compared to the $Sgcg^{-/-}$ nontreated hind limbs (Figure 8), comparable to previous literature.[18]

Magnitude of Effect Size Is Comparable Between NIR Optical Imaging and MRI

Cohen *d* values were calculated to determine the magnitude of effect size of NIR optical imaging versus MRI-T_2. Near-infrared optical imaging demonstrated comparable ability to differentiate control from *mdx* and $Sgcg^{-/-}$ mice, the ability of eccentric downhill treadmill running to induce damage to older *mdx* mice, and the restorative capabilities of AAV therapy in $Sgcg^{-/-}$ mice as compared to MRI-T_2 (Table 1). Importantly, both modalities demonstrated the statistically significant ability to detect changes in muscle damage, confirming the comparable abilities of NIR optical imaging and MRI to detect muscle pathology *in vivo*.
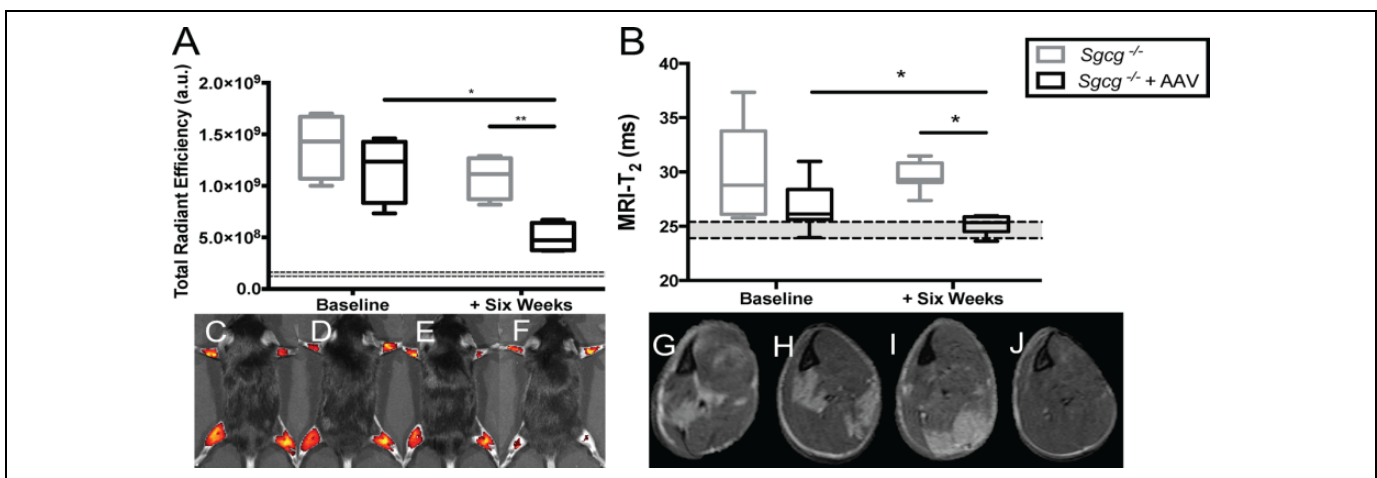
Figure 5. $Sgcg^{-/-}$ mice treated with *SGCG* loaded AAVs demonstrate decreased radiant efficiency and lower MRI-T_2 relaxation times following intervention. 6 weeks after intramuscular injections of an AAV containing human γ-sarcoglycan, total radiant efficiency was significantly decreased as compared to counterpart hindlimbs that did not received the AAV treatment (5A). Similarly, MRI demonstrated decreased T_2 values in the hindlimbs that were treated (5B). Baseline images of non-injected (5C) and to-be-treated (5D) mice were obtained as well as images after 6 weeks of mice with no treatment (5E) and treated (5F) mice. Visually note the increased fluorescence in the forelimbs (that were not treated) versus the treated hindlimbs of the AAV treated mouse in Figure 5E. Representative MR images shown in 5G-J, parallel to 5C-F. In 5A and 5B, the 95th percentile of healthy control mouse values are shown by the gray box. Statistical significance (*$p < 0.05$ and **$p < 0.01$) is shown.
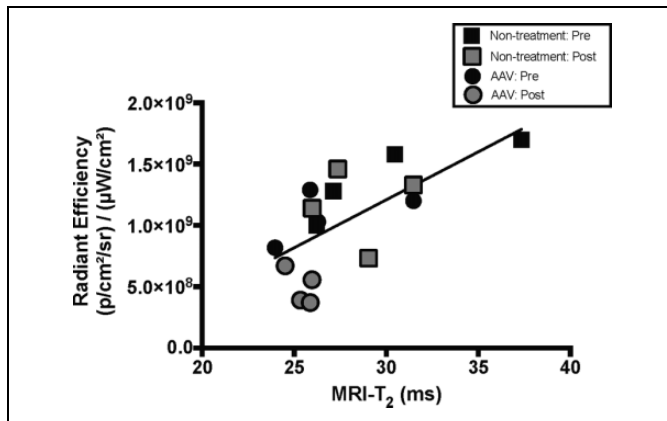
Figure 6. Increased total radiant efficiency correlates with increased magnetic resonance measures in $Sgcg^{-/-}$ mice with and without restorative AAV therapy. Mice that did and did not receive corrective therapy demonstrated correlative NIR optical imaging and MRI-T$_2$ ($r^2 = 0.43$, $p < 0.01$) data.

Discussion

The main aim of this investigation was to evaluate the efficacy of ICG-enhanced NIR optical imaging to detect and quantify muscle pathology caused by natural disease progression. Several experiments were performed to accomplish these tasks, including (1) a cross-sectional comparison between dystrophic and unaffected mice, (2) exacerbating muscle damage in a dystrophic phenotype by an eccentric treadmill running protocol, and (3) mitigation of disease through AAV delivery of the missing gene in $Sgcg^{-/-}$ mice. *Mdx* and $Sgcg^{-/-}$ mice demonstrated higher radiant efficiency values than healthy counterparts, indicating uptake of ICG into damaged muscles, with additional confirmation provided by MRI-T$_2$. Additional insult to muscle was implemented through an eccentric loading downhill treadmill running protocol, with quantitative visualization of muscle pathology provided by NIR optical imaging and MRI. Finally, an AAV encoding human SG was used to correct the gene deficiency in $Sgcg^{-/-}$ mice, with confirmation of successful treatment provided by the imaging modalities and histological assessment.

To our knowledge, we are the first group to demonstrate the ability of unmodified ICG-enhanced NIR optical imaging to detect perturbations to muscle health in the muscular dystrophies. To date, two groups have utilized contrast-enhanced NIR optical imaging to detect muscle damage in preclinical models with other NIR visible agents. Baudy et al elegantly demonstrated that a caged NIR cathepsin B substrate could be used to sensitively visualize damage, inflammation, regeneration, and response to therapy within dystrophic skeletal muscle in *mdx* mice.[44] In a rat model of acute muscle trauma, Inage et al utilized a modified ICG conjugate to observe muscle damage.[45] Our group previously showed the ability of unmodified ICG-enhanced NIR optical imaging to assess acute muscle damage in nondystrophic mice.[32] As unmodified ICG-enhanced NIR optical imaging has not been previously utilized to quantify and assess muscle pathology in the muscular dystrophies, we sought to demonstrate differentiation in fluorescent signal between unaffected control mice and 2 dystrophic mouse models, *mdx* and $Sgcg^{-/-}$ mice, indicating uptake of ICG into damaged sarcolemma (Figure 1A). Further confirmation of muscle pathology was demonstrated through several MR measures, such as MRI-T$_2$ (Figure 1B). Elevated MRI-T$_2$ relaxation times indicate damage and inflammation that occurs as a result of decreased membrane stability in dystrophic mice, as previously demonstrated.[46-48] Importantly, ICG-enhanced NIR optical imaging of multiple mice could be performed in less than 5 minutes, whereas comparable MRI data collection usually takes 30 to 60 minutes to perform per mouse. To determine whether these 2 modalities agreed, data were plotted against
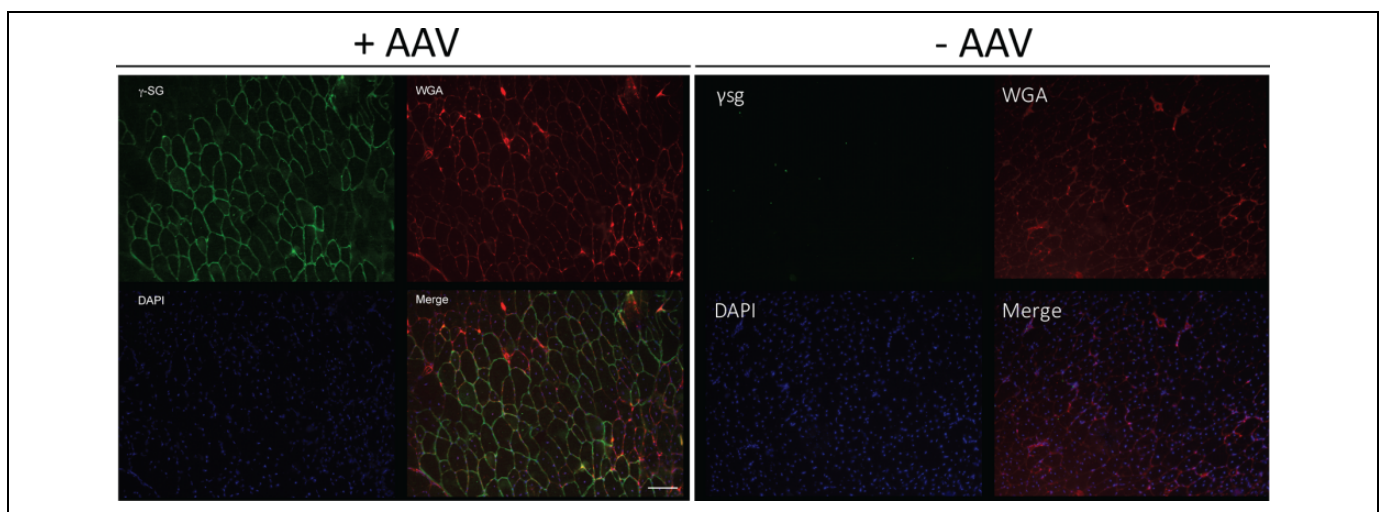
Figure 7. Immunofluorescence reveals restoration of γ-sarcoglycan in treated muscle. Representative TA sections that received (left panel) and did not receive (right panel) *SGCG* loaded AAVs are shown, stained for γ-sarcoglycan (green), wheat germ aggluttinin (red), and DAPI (blue), along with composite images. Scale bar is 100 μm.
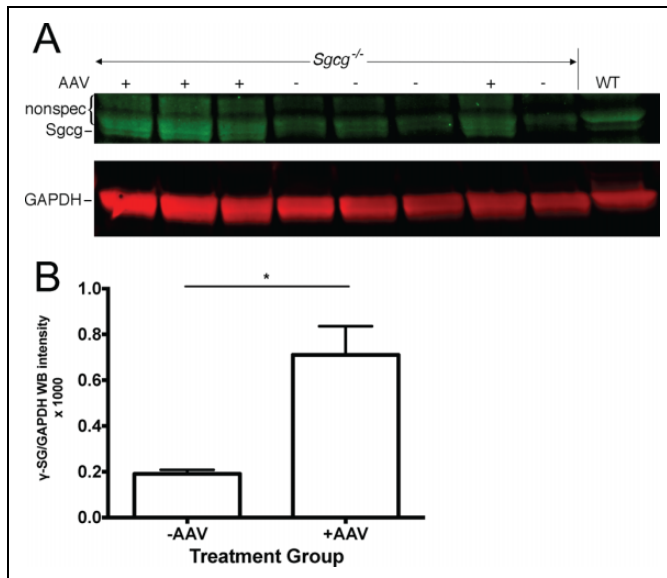
Figure 8. Expression of γ-sarcoglycan / GAPDH is present in the AAV treated hindlimbs of supports non-invasive markers of $Sgcg^{-/-}$ mice. Raw western blots (A) are shown for $Sgcg^{-/-}$ and wild type mice. The γ-sarcoglycan / GAPDH ratio is significantly increased in limbs treated with desAAV8hSGCG, as compared to limbs non-treated $Sgcg^{-/-}$ limbs (*$p < 0.01$).

Table 1. Effect Size Magnitude Demonstrates Comparable Differences Between NIR Optical Imaging and MR Measures.[a]

	NIR Optical Imaging	MRI-T_2
Control versus *mdx*	2.69	3.88
Control versus $Sgcg^{-/-}$	2.26	3.56
Treadmill-induced damage	2.06	.84
AAV restorative therapy	2.75	.97

Abbreviations: MRI, magnetic resonance imaging; NIR, near infrared.
[a]Cohen d effect size values for radiant efficiency and MRI-T_2 are presented, demonstrating comparable effect sizes for both modalities.

each other, and significant correlations were drawn between NIR optical imaging and MRI-T_2 when examining healthy and diseased muscles (Figure 2).

Optical imaging detected muscle damage in dystrophic muscle following downhill treadmill running. In addition to differentiating between control and dystrophic muscle, we determined whether optical imaging could be used to detect acutely induced muscle damage against a background of chronic disease induced damage. This is important in that as the muscular dystrophies are progressive by nature and constantly undergoing muscle turnover. Worsening of muscle pathology in a dystrophic phenotype was able to be investigated through a downhill treadmill running protocol, which is known to cause additional muscle damage due to eccentric loading damage to muscles during exercise.[31] When comparing data before and after treadmill running, mice demonstrated a significant increase in fluorescent dye uptake into the muscles (Figure 3A). Interestingly, MRI-T_2 did not show significant

differences in the forelimb and hind limb muscles when considered as a whole (Figure 3B) but did when individual muscle compartments were analyzed (Supplemental Figure 9, the forelimb posterior Figure 9B) compartment and hind limb medial (Supplemental Figure 9D) compartments in agreement with previous literature.[31] The lack of robustly elevated T_2 in the remaining compartments may be due to differences in biomechanical loading from the downhill treadmill exercises and heterogeneous distribution of disease in dystrophic muscle. Unexpectedly, a significant correlation was not observed when comparing T_2 to radiant efficiency before and after treadmill running (Figure 4). While subjectively one can separate pre-versus posttreadmill running, a clear correlation was not observed, potentially due to the assessment of whole limbs (fore- and hind-) rather than specific muscle groups. Consistent with previous reports,[31] MRI-T_2 revealed that not all the muscles are affected to the same extent following treadmill running and change in this case the optical signal may be diluted by muscles. Whereas these results demonstrate the sensitivity of optical imaging, they also highlight the high resolution that is afforded by MRI to look at muscle specific changes.

Perhaps, the most critical task of an outcome measure is to be able to detect changes following therapeutic intervention. In this study, we utilized ICG-enhanced NIR optical imaging and MRI to demonstrate the mitigation of LGMD-2C through restoration of γ-sarcoglycan through intramuscular injections of desAAV8hSGCG (Figure 5). Supporting these findings are the data demonstrating modest longitudinal correlation of radiant efficiency and MRI-T_2 (Figure 6) and histological immunofluorescence confirmation of γ-sarcoglycan restoration in mice treated with desAAV8hSGCG (Figures 7 and 8) following AAV treatment. Whereas we have used the dystrophic mice to demonstrate the potential of optical imaging, future studies in humans are warranted. Indeed, it has previously been shown that a combined MRI and ICG-enhanced optical imaging can be used to stage human breast cancer.[38] As elegantly demonstrated by Ntziachristos and colleagues, coregistered gadolinium-enhanced MRI and ICG-enhanced diffuse optical tomography images of breast tumors were able to be obtained, demonstrating the capability of ICG-enhanced optical imaging to accurately and safely be implemented in humans.[38] Importantly, the methodologies utilized in this study to observe this correction of disease are implementable in both preclinical and clinical models, potentially accelerating the translation of therapies to the clinic.

Both minimally invasive technologies, NIR optical imaging and MRI, demonstrate adequate competency to detect disease-induced pathology, further insult to muscle, and correction of disease pathology in muscle (Table 1). Advantages and disadvantages exist when using either technology—MRI provides superior soft tissue spatial resolution, while NIR optical imaging demonstrates the ability to sensitively assess changes to sarcolemmal integrity in an *in vivo* manner. Typically, to assess the integrity of sarcolemmal membranes, a blood pooling dye such as Evans blue dye is administered, prior to sacrifice and extraction of the muscle.[49] In our study, we demonstrate the

ability to assess sarcolemmal integrity in an *in vivo* manner by using ICG-enhanced NIR optical imaging. Interestingly, following desAAV8hSGCG restoration in $Sgcg^{-/-}$ mice (Figure 5), MRI-T_2 returns to control levels (indicated by the dashed gray boxes in Figure 5), but NIR optical imaging data do not return to baseline levels. This may be due to several reasons, including incomplete disease correction by desAAV8hSGCG, as muscle had already become too fibrotic prior to desAAV8hSGCG therapy limiting the distribution of therapy throughout the diseased muscle, or that residual ICG remained trapped in the muscle. Overall, these conflicting findings suggest that NIR optical imaging and MR are complementary, rather than supplementary technologies. Each technique provides valuable information; MRI provides better spatial discrimination, while NIR optical imaging provides quicker, cheaper, and comparably sensitive differentiation of pathologic states of muscle.

As clinical trials continue to press forward with suboptimal results, we are reminded of the importance of having sufficient outcome measures that are able to detect natural progression of disease and therapeutic efficacy in safe, minimally invasive, objective, repeatable, and quantifiable manners.[50-53] A recent shift toward quantitative MRI has drawn excitement, as a great deal of information regarding natural progression of the muscular dystrophies[50,54] and response to treatment[55] can be obtained. Additionally, data can continue to be collected following the inevitable loss of ambulation in these populations. Building upon MRI as a well-proven imaging modality, ICG-enhanced NIR optical imaging demonstrates that we can quantitatively assess muscle pathology in a safe, repeatable, and minimally invasive fashion, complementing the findings of the more expensive and time-consuming MR procedures.

In this study, we demonstrate the development of ICG-enhanced NIR optical imaging to assess the state of muscle health, but this study is not without limitations. First, ICG is a nonspecific contrast agent, which is both an advantage and disadvantage. It may be advantageous to use because it can ubiquitously be applied for several different applications in and beyond muscle. For the same reasons, this may be viewed as a disadvantage, as it is taken up nonspecifically anywhere where there may be a compromised membrane. Although NIR optical imaging was deemed to be comparable to MRI by effect size measurements, the development of technology to provide better spatial resolution (ie, assessment in different planes) would provide much benefit to NIR imaging. Additionally, while this study elicited the ability to differentiate dystrophic and repaired muscle in a cross-sectional manner, longitudinal studies may allow for monitoring of subtle disease progression or regression. Utilizing NIR optical imaging to assess the efficacy between different disease-modifying techniques for the muscular dystrophies, such as DNA replacement, RNA manipulation, decreasing inflammation and fibrosis, and correcting blood flow perturbations would be worthwhile investigations. Lastly, Western blotting for γ-sarcoglycan is made difficult due to the commercial antibodies which have residual background binding. Future studies warrant the development of standardized protocols to longitudinally investigate muscular dystrophies and using other disease-modifying agents, determining whether NIR optical imaging can similarly detect amelioration of disease both in preclinical and clinical models. Certainly, much more developmental work is required before contrast-enhanced NIR optical imaging can provide a meaningful alternative to MRI.

In summary, we demonstrate the utilization of NIR optical imaging with an FDA-approved NIR fluorophore, ICG, to assess and quantify pathology resulting from two different muscular dystrophies in mice, worsening of muscle pathology through eccentric loading, as well as correction of disease through an AAV restorative therapy. Because of its comparable power to identify muscle pathology to MRI, ICG-enhanced NIR optical imaging may serve as a multipurpose, minimally invasive, safe imaging technology that can be applied to other disorders of muscle in both animals and humans, available for rapid translation to clinical trials.

Supplemental Material

Supplementary material for this article is available online.

References

1. Flanigan KM. The muscular dystrophies. *Semin Neurol*. 2012; 32(3):255–263.
2. Kang PB, Griggs RC. Advances in muscular dystrophies. *JAMA Neurol*. 2015;72(7):741–742.
3. Mah JK, Korngut L, Dykeman J, Day L, Pringsheim T, Jette N. The muscular dystrophies. *Semin Neurol*. 2012;32(3):255–263.
4. Kang PB, Griggs RC. Dystrophin: the protein product of the Duchenne muscular dystrophy locus. *Cell*. 1987;51(6):919–928.
5. Ervasti JM, Campbell KP. Membrane organization of the dystrophin-glycoprotein complex. *Cell*. 1991;66(6):1121–1131.

6. McNally EM, Passos-Bueno MR, Bönnemann CG, et al. Mild and severe muscular dystrophy caused by a single gamma-sarcoglycan mutation. *Am J Hum Genet*. 1996;59(5):1040–1047.

7. Barton ER. Impact of sarcoglycan complex on mechanical signal transduction in murine skeletal muscle. *Am J Physiol Cell Physiol*. 2006;290(2): C411–C419.

8. Syed YY. Eteplirsen: first global approval. *Drugs*. 2016;76(17): 1699–1704.

9. Haas M, Vlcek V, Balabanov P, et al. European medicines agency review of ataluren for the treatment of ambulant patients aged 5 years and older with Duchenne muscular dystrophy resulting from a nonsense mutation in the dystrophin gene. *Neuromuscul Disord*. 2015;25(1):5–13.

10. Traynor K. Deflazacort approved for Duchenne muscular dystrophy. *Am J Health Syst Pharm*. 2017;74(6):368.

11. Hoy SM. Nusinersen: first global approval. *Drugs*. 2017;77(4): 473–479.

12. Hack AA, Ly CT, Jiang F, et al. Gamma-sarcoglycan deficiency leads to muscle membrane defects and apoptosis independent of dystrophin. *J Cell Biol*. 1998;142(5):1279–1287.

13. Sicinski P, Geng Y, Ryder-Cook AS, Barnard EA, Darlison MG, Barnard PJ. The molecular basis of muscular dystrophy in the mdx mouse: a point mutation. *Science*. 1989;244(4912):1578–1580.

14. Anderson JE, McIntosh LM, Poettcker R. Deflazacort but not prednisone improves both muscle repair and fiber growth in diaphragm and limb muscle in vivo in the mdx dystrophic mouse. *Muscle Nerve*. 1996;19(12):1576–1585.

15. Barton ER, Morris L, Kawana M, Bish LT, Toursel T. Systemic administration of L-arginine benefits mdx skeletal muscle function. *Muscle Nerve*. 2005;32(6):751–760.

16. Goyenvalle A, Griffith G, Babbs A, et al. Functional correction in mouse models of muscular dystrophy using exon-skipping tricyclo-DNA oligomers. *Nat Med*. 2015;21(3):270–275.

17. Matsuo M, Masumura T, Nishio H, et al. Exon skipping during splicing of dystrophin mRNA precursor due to an intraexon deletion in the dystrophin gene of Duchenne muscular dystrophy kobe. *J Clin Invest*. 1991;87(6):2127–2131.

18. Barton ER. Restoration of gamma-sarcoglycan localization and mechanical signal transduction are independent in murine skeletal muscle. *J Biol Chem*. 2010;285(22):17263–17270.

19. Barton-Davis ER, Cordier L, Shoturma DI, Leland SE, Sweeney HL. Aminoglycoside antibiotics restore dystrophin function to skeletal muscles of mdx mice. *J Clin Invest*. 1999;104(4): 375–381.

20. McDonald AA, Hebert SL, Kunz MD, Ralles SJ, McLoon LK. Disease course in mdx: utrophin+/- mice: comparison of three mouse models of Duchenne muscular dystrophy. *Physiol Rep*. 2015;3(4). pii: e12391.

21. Vohra RS, Mathur S, Bryant ND, Forbes SC, Vandenborne K, Walter GA. Age-related T2 changes in hindlimb muscles of mdx mice. *Muscle Nerve*. 2016;53(1):84–90.

22. Hakim CH, Wasala NB, Duan D. Evaluation of muscle function of the extensor digitorum longus muscle ex vivo and tibialis anterior muscle in situ in mice. *J Vis Exp*. 2013;(72). pii: 50183.

23. Goemans N, Klingels K, van den Hauwe M, et al. Six-minute walk test: reference values and prediction equation in healthy boys aged 5 to 12 years. *PLoS One* [Internet]. 2013;8(12). http://www.ncbi.nlm.nih.gov/pmc/articles/PMC3877199/. Accessed May 11, 2017.

24. Cacchiarelli D, Legnini I, Martone J, et al. miRNAs as serum biomarkers for Duchenne muscular dystrophy. *EMBO Mol Med*. 2011;3(5):258–265.

25. Carlier PG, Mercuri E, Straub V. Applications of MRI in muscle diseases. *Neuromuscul Disord NMD*. 2012;22(suppl 2):S41.

26. Dunn JF, Zaim-Wadghiri Y. Quantitative magnetic resonance imaging of the mdx mouse model of Duchenne muscular dystrophy. *Muscle Nerve*. 1999;22(10):1367–1371.

27. Finanger EL, Russman B, Forbes SC, Rooney WD, Walter GA, Vandenborne K. Use of skeletal muscle MRI in diagnosis and monitoring disease progression in Duchenne muscular dystrophy. *Phys Med Rehabil Clin N Am*. 2012;23(1):1–10, ix.

28. Forbes SC, Willcocks RJ, Rooney WD, Walter GA, Vandenborne K. MRI quantifies neuromuscular disease progression. *Lancet Neurol*. 2016;15(1):26–28.

29. Hollingsworth KG, Garrood P, Eagle M, Bushby K, Straub V. Magnetic resonance imaging in Duchenne muscular dystrophy: longitudinal assessment of natural history over 18 months. *Muscle Nerve*. 2013;48(4):586–588.

30. Eresen A, McConnell S, Birch SM, Griffin JF, Kornegay JN, Ji JX. Localized MRI and histological image correlation in a canine model of Duchenne muscular dystrophy. *Conf IEEE Eng Med Biol Soc*. 2016;2016:4083–4086.

31. Mathur S, Vohra RS, Germain SA, et al. Changes in muscle T2 and tissue damage after downhill running in mdx mice. *Muscle Nerve*. 2011;43(6):878–886.

32. Chrzanowski SM, Batra A, Lee-McMullen B, et al. Near-infrared optical imaging noninvasively detects acutely damaged muscle. *Am J Pathol*. 2016;186(10):2692–2700.

33. Fan RH, Does MD. Compartmental relaxation and diffusion tensor imaging measurements in vivo in λ-carrageenan-induced edema in rat skeletal muscle. *NMR Biomed*. 2008;21(6):566–573.

34. Elder CP, Apple DF, Bickel CS, Meyer RA, Dudley GA. Intra-muscular fat and glucose tolerance after spinal cord injury—a cross-sectional study. *Spinal Cord*. 2004;42(12):711–716.

35. Bo Li Z, Zhang J, Wagner KR. Inhibition of myostatin reverses muscle fibrosis through apoptosis. *J Cell Sci*. 2012;125(pt 17): 3957–3965.

36. Brockmann MA, Kemmling A, Groden C. Current issues and perspectives in small rodent magnetic resonance imaging using clinical MRI scanners. *Methods San Diego Calif*. 2007;43(1):79–87.

37. Raabe A, Beck J, Gerlach R, Zimmermann M, Seifert V. Near-infrared indocyanine green video angiography: a new method for intraoperative assessment of vascular flow. *Neurosurgery*. 2003; 52(1):132–139; discussion 139.

38. Ntziachristos V, Yodh AG, Schnall M, Chance B. Concurrent MRI and diffuse optical tomography of breast after indocyanine green enhancement. *Proc Natl Acad Sci*. 2000;97(6):2767–2772.

39. Zelken JA, Tufaro AP. Current trends and emerging future of indocyanine green usage in surgery and oncology: an update. *Ann Surg Oncol*. 2015;22(suppl 3):S1271–S1283.

40. Guenette JA, Henderson WR, Dominelli PB, et al. Blood flow index using near-infrared spectroscopy and indocyanine green as

a minimally invasive tool to assess respiratory muscle blood flow in humans. *Am J Physiol Regul Integr Comp Physiol*. 2011; 300(4):R984–R992.

41. Frangioni JV. In vivo near-infrared fluorescence imaging. *Curr Opin Chem Biol*. 2003;7(5):626–634.

42. Weissleder R, Ntziachristos V. Shedding light onto live molecular targets. *Nat Med*. 2003;9(1):123–128.

43. Weissleder R. A clearer vision for in vivo imaging. *Nat Biotechnol*. 2001;19(4):316–317.

44. Baudy AR, Sali A, Jordan S, et al. Non-invasive optical imaging of muscle pathology in mdx mice using cathepsin caged near-infrared imaging. *Mol Imaging Biol*. 2011;13(3):462–470.

45. Inage K, Sakuma Y, Yamauchi K, et al. Longitudinal evaluation of local muscle conditions in a rat model of gastrocnemius muscle injury using an in vivo imaging system. *J Orthop Res*. 2015;33(7): 1034–1038.

46. McIntosh LM, Baker RE, Anderson JE. Magnetic resonance imaging of regenerating and dystrophic mouse muscle. *Biochem Cell Biol*. 1998;76(2-3):532–541.

47. Pacak CA, Walter GA, Gaidosh G, et al. Long-term skeletal muscle protection after gene transfer in a mouse model of LGMD-2D. *Mol Ther*. 2007;15(10):1775–1781.

48. Walter G, Cordier L, Bloy D, Sweeney HL. Noninvasive monitoring of gene correction in dystrophic muscle. *Magn Reson Med*. 2005;54(6):1369–1376.

49. Hamer PW, McGeachie JM, Davies MJ, Grounds MD. Evans blue dye as an in vivo marker of myofibre damage: optimising parameters for detecting initial myofibre membrane permeability. *J Anat*. 2002;200(1):69–79.

50. Bonati U, Hafner P, Schädelin S, et al. Quantitative muscle MRI: a powerful surrogate outcome measure in Duchenne muscular dystrophy. *Neuromuscul Disord NMD*. 2015;25(9):679–685.

51. Henricson EK, Abresch RT, Cnaan A, et al. The cooperative international neuromuscular research group Duchenne natural history study: glucocorticoid treatment preserves clinically meaningful functional milestones and reduces rate of disease progression as measured by manual muscle testing and other commonly used clinical trial outcome measures. *Muscle Nerve*. 2013;48(1): 55–67.

52. Kinali M, Arechavala-Gomeza V, Cirak S, et al. Muscle histology vs MRI in Duchenne muscular dystrophy. *Neurology*. 2011;76(4): 346–353.

53. Taylor LE, Kaminoh YJ, Rodesch CK, Flanigan KM. Quantification of dystrophin immunofluorescence in dystrophinopathy muscle specimens. *Neuropathol Appl Neurobiol*. 2012;38(6):591–601.

54. Hollingsworth KG. Quantitative MRI in muscular dystrophy: an indispensable trial endpoint? *Neurology*. 2014;83(11):956–957.

55. Arpan I, Willcocks RJ, Forbes SC, et al. Examination of effects of corticosteroids on skeletal muscles of boys with DMD using MRI and MRS. *Neurology*. 2014;83(11):974–980.